Journal of Theoretical and Applied Physics (JTAP), Vol.16, No. 4, 162235 (1-8), 2022
Received 14 April 2022 ; Accepted 31 July 2022 ; [http://dx.doi.org/10.30495/jtap.162235]

The dynamics of plasmoid instability in the presence of asymmetric parallel shear flow

Hossein Lotfi, Mahboub Hosseinpour*

Abstract
The nonlinear evolution of the magnetic reconnection and onset of the plasmoid instability are investigated by using 2.5-dimensional MHD simulations when the sheared plasma flow is anti-symmetric on either side of the boundary layer. In particular, we considered a wide range of velocity amplitude of shear flow (V_0) (from sub-Alfvénic to level of super-Alfvénic) and the shear flow scale length (a_v) compared to equilibrium magnetic field scale length (a_B). We found that sub-Alfvénic shear flows (here $V_0 \leq 0.6V_A$) can change the O-point position of magnetic islands. The plasmoid instability is suppressed with increasing shear flow velocity, and the Kelvin-Helmholtz instability appears instead of the plasmoid instability when the shear flow is of the order of the Alfvénic or larger. Thus, at the limit of Alfvénic velocity, the magnetic field lines twist near the magnetic reconnection site due to the presence of asymmetric shear flows. The shear flow scale length (or shear flow thickness) can have either stabilization or destabilization effects on the current sheet development. For sub-Alfvénic shear flow (here $V_0 \leq 0.8V_A$), $a_v < a_B$ has a suppressing effect on the plasmoid instability, while $a_v > a_B$ has a boosting effect on the plasmoid instability. Therefore, we found a critical value for the shear flow thickness that magnetic reconnection has the maximum value. The boosting effect of the shear flow on the current sheet becomes strongest at $a_{vc} = 1.2a_B$.

Keywords
Plasmoid instability, Magnetic reconnection, MHD simulation, Space plasmas.

Faculty of Physics, University of Tabriz, Tabriz, Iran.
***Corresponding author**: hosseinpour@tabrizu.ac.ir

1. Introduction

Resistive magnetohydrodynamic (MHD) instabilities such as plasmoid instability (PI) [1] and Kelvin-Helmholtz instability (KHI) [2] are two important macroscopic instabilities in laboratory and space plasmas. These instabilities occur in highly conductive and magnetized plasmas during the magnetic reconnection process in a narrow current layer. Magnetic reconnection is a fundamental process in space and laboratory plasma physics [3,4] in which magnetic field lines are merged, cut, and reconnected. During magnetic reconnection events, the stored magnetic energy in plasma is rapidly released and converted into kinetic energy and plasma heating. It has been widely used to explain explosive events and fast energy transformation phenomena, such as solar flares [5], coronal mass ejections [6], and the interaction of solar wind with Earth's magnetosphere [7].

Any change in plasma parameters can have significant effects on the magnetic reconnection process and the non-linear evolution of the PI. Plasmoid formation occurs when the Lundquist number based on the system size $S_L = L_x V_A/\eta$, where L_x is the reconnection layer length, V_A is the Alfvén speed and η is the resistivity, exceeds a critical value S_c. The most commonly critical Lundquist number value is $S_c \approx 10^4$ [8–10]. A large number of studies, commonly computational, have considered the role of main plasma parameters on the magnetic reconnection and the PI, such as the plasma-β [11–13], plasma viscosity [14, 15], non-uniform resistivity [16], asymmetric magnetic field and plasma mass density in two sides of the reconnection current sheet [17, 18], and presence of magnetic field perpendicular to the reconnection plane (i.e, guide field) [19]. Additionally, plasma flow is common in space and laboratory plasmas. The presence of any plasma flow can play an essential role in the structure of the current sheet and the PI dynamics during the magnetic reconnection.

Different kinds of flows such as diamagnetic flow, out-of-plane shear flow, streaming flow, and parallel shear flow have been proven in plasmas. The influence of each of these flows on the tearing mode instability (TMI) and reconnection layer structure has been studied. The influences of shear flow out of the magnetic reconnection plane in 2D simulations have been investigated [20, 21]. They found that the shear flow perpendicular to the reconnection plane can change the quadrupole structure of the out-of-plane magnetic field and therefore modify the magnetic reconnection rate. Also, in the Earth's magnetotail, the presence of the bulk plasma flows parallel to the current sheet are commonly observed in the plasma sheet [22, 23]. The existence of a streaming plasma flow in the current sheet may have a considerable effect on the tearing mode instability [24–26]. They concluded that the

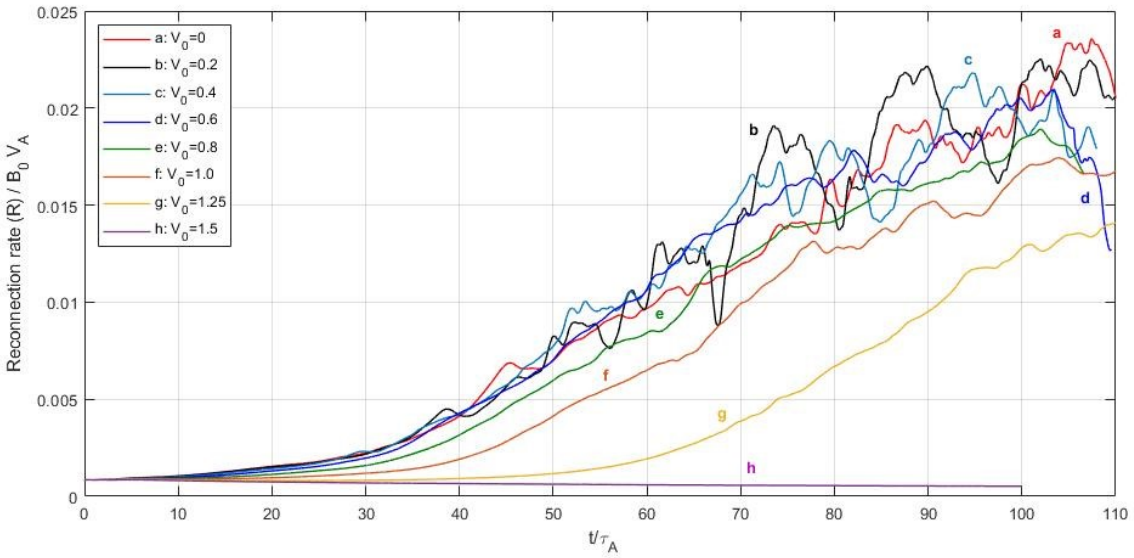

Figure 1. Temporal evolution of the magnetic reconnection rate for different values of the shear flow velocity amplitude.

growth rate of the tearing mode instability is larger than that without a streaming flow. The presence of sheared plasma flows is observed in many Astrophysics situations. Shear flows exist naturally in many physical phenomena, such as solar flares [27–29], erupting arcade [30], and in the current sheet at the dayside magnetopause is created due to the interaction of the solar wind magnetic field with that of the Earth's magnetosphere which is in the opposite directions [31, 32].

Numerically, the dynamic effect of the symmetric parallel shear flows on the evolution of the resistive tearing mode [33, 34] and PI [35, 36] have been studied in the past few decades. The influences of super-Alfvénic flow and sub-Alfvénic flow on the PI and tearing modes are very different. The KH instability can be induced in the presence of the super-Alfvénic flow velocity with a time scale of the order of ten Alfvénic times, while the time scale of the resistive tearing modes or plasmoid instability with the sub-Alfvénic shear flow is of the order of hundred Alfvénic times [37]. In the lack of shear flow, when the current sheet becomes unstable to the PI, the large plasmoids (or magnetic islands) are formed in the current sheet through the magnetic reconnection process. However, in the presence of parallel shear flows, the magnetic reconnection rate and rate of the plasmoid formation decreased with an increase in shear flow amplitude up to the critical value, after which the PI transients to the KH instability. This critical value of share flow amplitude is Alfvén velocity for a resistive MHD model. In general, the shear flow stabilizes the PI. However, recently Hosseinpour et al [35] found that the symmetry shear flow can trigger PI when the shear flow thickness is greater than the current sheet thickness.

However, little attention has been paid to the role of shear flow on the nonlinear evolution of PI at compressible plasmas. In this paper, we aim to study the dynamics of PI and the nonlinear development of the current layer in the presence of an initially asymmetric shear flow parallel to the magnetic field. Thus, we will consider both the effects of shear flow velocity amplitude and shear flow scale length. The paper is arranged as follows: numerical setup and equations are defined in section 2. The simulation results are presented in section 3. In section 4, we will give a summary and conclusion.

Table 1. Shear flow velocity amplitude at up and down of the current sheet.

V_0(Velocity amplitude)	$V_{0,Upstream}$	$V_{0,Downstream}$
0	0	0
0.2	0.2	-0.13
0.4	0.4	-0.26
0.6	0.6	-0.4
0.8	0.8	-0.53
1.0	1.0	-0.66
1.25	1.25	-0.83
1.5	1.5	-1.0

2. Model and Method

For investigation of the effect of asymmetric shear flow on the plasmoid instability dynamics, we use a finite-volume 2.5D resistive MHD code, Open MHD code, which was developed by Zenitani [38]. Numerical fluxes are estimated by an HLLD approximate Riemann solver [39]. The second-order TVD Runge-Kutta time marching method is used, and also, the hyperbolic divergence cleaning method ($\nabla \cdot \mathbf{B} = 0$) is employed for the solenoidal condition [40]. The basic one-fluid compressible resistive MHD equations that are solved by using

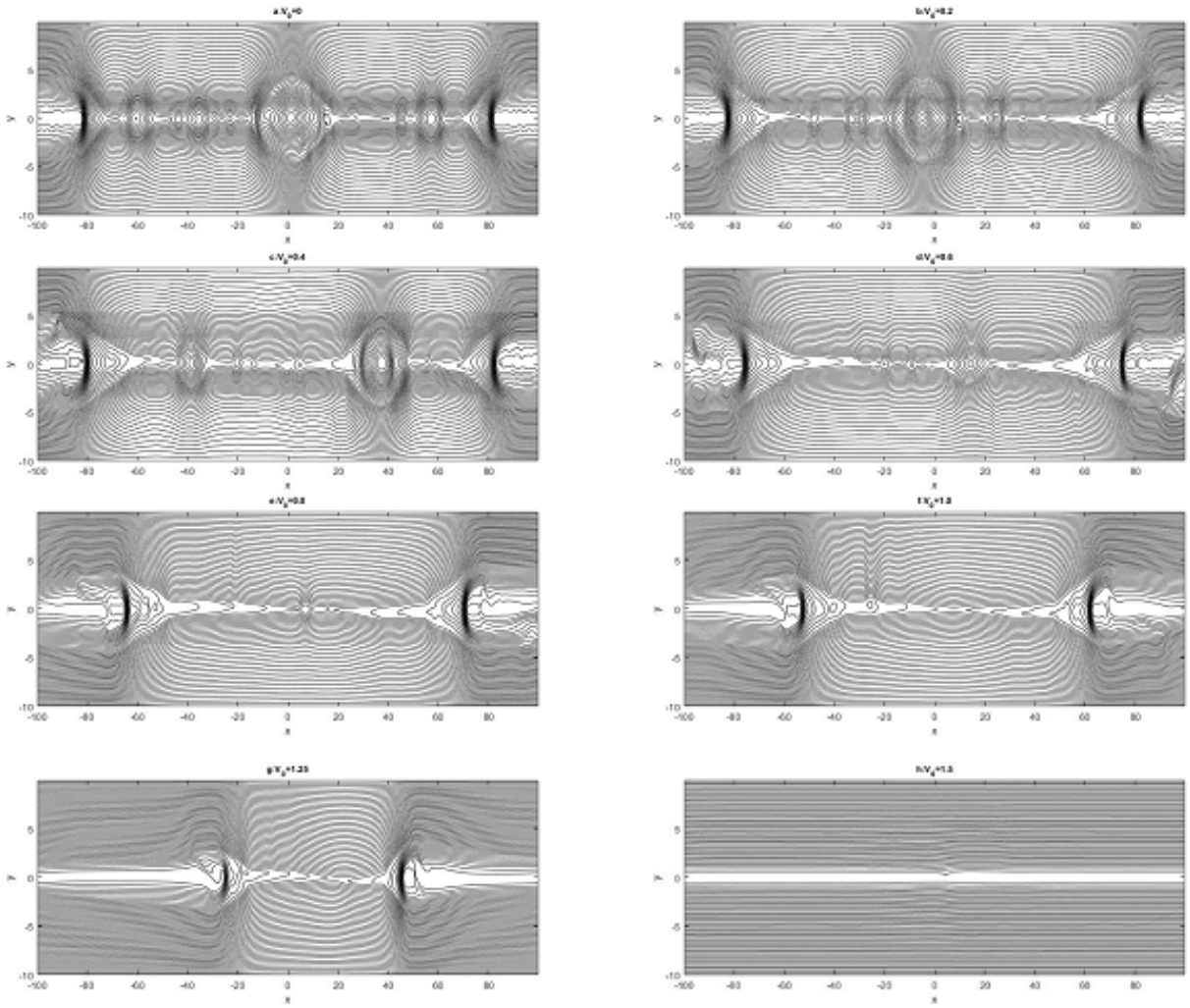

Figure 2. Variation of magnetic field lines at the same time, $t = 100\tau_A$, for different values of the shear flow velocity amplitude.

OpenMHD code in a cartesian geometry system are as follows: The continuity equation

$$\frac{\partial \rho}{\partial t} + \nabla \cdot (\rho \mathbf{V}) = 0 \tag{1}$$

where ρ is plasma mass density, and $\mathbf{V}$ is plasma flow velocity; the Euler equation

$$\frac{\partial (\rho \mathbf{V})}{\partial t} + \nabla \cdot [\rho \mathbf{V}\mathbf{V} + (p + \frac{B^2}{2})\mathbf{I} - \mathbf{B}\mathbf{B}] = 0 \tag{2}$$

where p is the gas pressure, $\mathbf{B}$ is the magnetic field, and $\mathbf{I}$ is unit tensor; the energy equation

$$\frac{\partial e}{\partial t} + \nabla \cdot ((e + p + \frac{B^2}{2})\mathbf{V} - (\mathbf{V} \cdot \mathbf{B})\mathbf{B} + \eta \mathbf{j} \times \mathbf{B}) = 0 \tag{3}$$

where $e = p/(\gamma - 1) + \rho V^2/2 + B^2/2$ is total energy density, η is electrical resistivity, and j is the current density; the induction equation

$$\frac{\partial \mathbf{B}}{\partial t} + \nabla \cdot (\mathbf{V}\mathbf{B} - \mathbf{B}\mathbf{V}) + \nabla \times (\eta j) = 0 \tag{4}$$

and ohm's law

$$\mathbf{E} + \mathbf{V} \times \mathbf{B} = \eta j \tag{5}$$

where $\mathbf{E}$ is electrical field. We set the specific heat ratio $\gamma = 5/3$. All variables are functions of space (x, y) and time (t), and also, the variation of variables in the z-direction is ignored $\partial/\partial z$. For the convenience of numerical computations, all variables are dimensionless. For example, $\mathbf{B}/B_0 \to \mathbf{B}$, $\rho/\rho_0 \to \rho$, $(p/B_0^2)/2\mu_0 \to p$, $\mathbf{V}/V_A \to \mathbf{V}$, $\mathbf{E}/B_0 V_A \to \mathbf{E}$, $\mathbf{j}/L_0 B_0 \to \mathbf{j}$, $t/\tau_A \to t$ and $\eta/L_0 V_A \to \eta$. Where $\tau_A (= a_B/V_A)$ is Alfvénic time and L_0 is the length scale of the system so that all spatial variables become normalized to it.

The simulations are performed in a rectangular box of size L_x=[-100,100] and L_y=[-10,10]. Here, x is the longitudinal

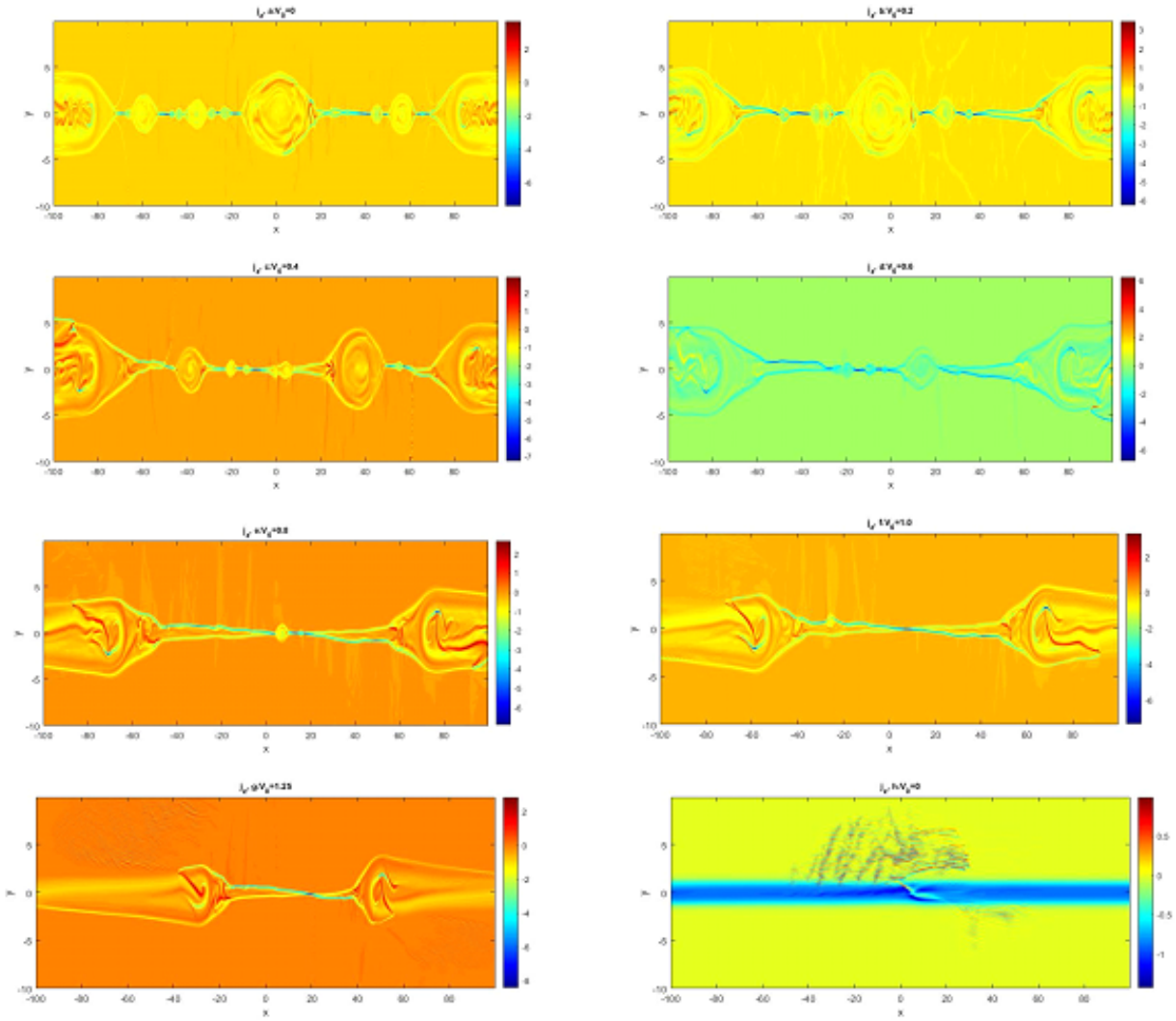

Figure 3. Out-of-plane current density for different values of shear flow amplitude at $t = 100\tau_A$ corresponding to figure2.

direction, and y is the normal direction to the reconnection plane, with 3200×320 cells. The numerical grid sizes are $\Delta x = \Delta y = 0.0625$, which is assumed uniform in space and constant in time. We consider the open boundary condition at the left ($x = -L_x$) and right ($x = L_x$) boundaries so that the reconnected field lines can cross through these boundaries freely. On the other hand, the conducting wall boundary condition is set at the bottom ($y = -L_y$) and top ($y = L_y$) boundaries, where the plasma cannot flow through these boundaries.

The magnetic field $\mathbf{B}$ and plasma flow velocity $\mathbf{V}$ can be represented as $B = \nabla\psi \times \hat{z} + B_z\hat{z}$ and $\mathbf{V} = \nabla\phi \times \hat{z} + v_z\hat{z}$ respectively, where ψ is the magnetic flux function, B_z is the magnetic field component perpendicular to the reconnection plane (guide field), ϕ is the stream function, and v_z is the flow speed in the $\hat{z}$ direction. Assuming $B_z = 0$ and $v_z = 0$, the initial magnetic field and asymmetric sheared plasma flow are given as follows:

$$B_x(y) = B_0 \tanh(\frac{y}{a_B}) \tag{6}$$

$$V_x(y) = V_0[\frac{\tanh(\frac{y}{a_v} - b) + b}{(1+b)}] \tag{7}$$

where $B_0 = 1.0$ and V_0 are the asymptotic values of the magnetic field and the shear flow velocity amplitude, respectively. $a_B = 0.7$, $b = 0.2$ and a_v are the half thickness of the current sheet, the velocity asymmetry parameter and shear scale length, respectively. By solving the condition of initial force-balanced equilibrium, the thermal pressure is given by $p = B_0^2/2(1 + \beta/2 - B_x^2)$, and assuming the initial thermal equilibrium condition, the plasma mass density is obtained by $\rho = p/1 + \beta$, where β is the plasma beta parameter, and its value is fixed to be 0.2 in this study.

In this simulation, according to Ref [41], initially, we use a non-uniform resistive disturbance during $0 < t < 5$ as $\eta = \eta_0 \exp(-x^2 - y^2)$ where $\eta_0 = 0.025$. This primary resistive disturbance leads to the formation of an X-point at the origin, that is, $x = y = 0$. After $t = 5$, the uniform resistiv-

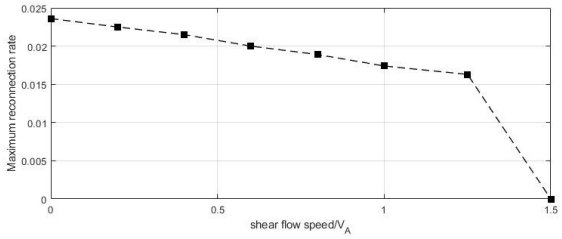

Figure 4. Maximum reconnection rate for different values of shear flow velocity with $a_v = a_B$.

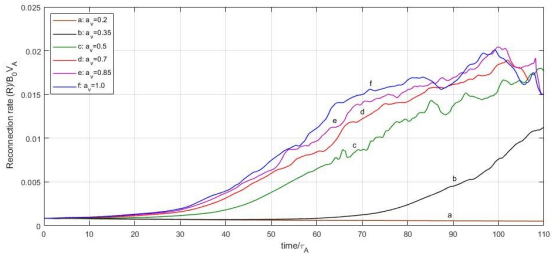

Figure 5. Temporal variation of magnetic reconnection rate for different values of half-thickness of shear flow with constant velocity amplitude $V_0 = 0.8$.

ity $\eta = 0.0015$ is supposed. Therefore, for this resistivity, the corresponding Lundquist number is estimated to be $s = L_x V_A/\eta$=231481, where V_A is taken to be 3.47.

3. Simulation Results

In this section, we aim to investigate the influence of asymmetric sheared plasma flow velocity amplitude and shear scale length on the growth rate of the plasmoid instability.

3.1 Varying shear flow velocity amplitude

At first, we examine the effect of shear flow with different values of velocity amplitude by keeping the shear scale length fixed at $a_v = a_B = 0.7$. In our study, a wide range of different values of shear flow velocities $V_0 = (0, 0.2, 0.4, 0.6, 0.8, 1.0, 1.25, 1.5)V_A$, from sub-Alfvénic to super-Alfvénic velocities is supposed. $V_0 = 0$ represents a case without shear flow, and $V_0 = 1.0$ represents a case with Alfvénic speed, which is the critical velocity in sheared plasma flow studies. Therefore, $V_0 > 1.0$ denotes the super-Alfvénic velocity, and $V_0 < 1.0$ denotes the sub-Alfvénic velocity. According to equation 7, the shear flow velocity amplitude in up-stream and down-stream of the boundary layer is shown in Table 1.

The magnetic reconnection rate for different values of shear flow velocity is shown in Figure 1. In plots of Figure 1, both linear and nonlinear regimes are clearly shown, so that for $V_0 \leq 0.6V_A$, linear and nonlinear phases of reconnection rate plots are independent of the shear flow amplitude. Also, by increasing the shear flow velocity amplitude $V_0 > 0.6V_A$, the nonlinear phase oscillations are suppressed, and the linear phase of the system is longer. Therefore, the formation of multiple reconnection sites in the current layer reduces, and the growth rate of plasmoid instability is suppresses. The magnetic reconnection does not occur in the current sheet when there is super-Alfvénic shear flow in the plasma, and the current sheet will have a stable state [35]. Contrary to this expectation, in the (g) plot of Figure 1, due to the asymmetric shear flow on both sides of the current sheet, the reconnection process can occur. Therefore, reconnection does not occur when the shear flow velocities on either side of the current sheet are of the order of Alfvénic speeds or larger (Fig.1(h)), and the current layer remains stable.

Now, to understand the evolution of the current sheet in the presence of sheared plasma flow, the variation of the force lines, which are the same as the magnetic field lines, at the same time, $t = 100\tau_A$, for different values of the velocity amplitude is shown in Figure 2. Figure 2(a) corresponds to a state in which there is no shear flow $V_0 = 0$, so the plasmoid instability sufficiently develops within the current sheet. As can be seen from Figure 2(b), a small amplitude of velocity does not have significant effect on the evolution of the current sheet and secondary plasmoids formation in the current sheet. As the shear flow velocity amplitude increases, the plasmoid growth rate slows down. This is evident from the size of the primary plasmoid in the center of the current layer in different panels in Figure 2. Also, the presence of shear flow leads to the advection of the primary plasmoid out towards boundaries. From (f) and (g) panels of Figure 2, we can see that the plasmoid instability is suppressed, and Kelvin-Helmholtz instability appears when the velocity magnitude is of the order of Alfvénic velocity or larger, while the velocity magnitude is of the order of the sub-Alfvénic velocity on one side of the current sheet. When the shear flow velocity magnitude on both sides of the current sheet is on the order of Alfvénic or greater, the current sheet will be stable against instability. This point can be seen in Figure 2(h) where $V_0 = 1.5$.

Furthermore, corresponding to the different panels of Figure 2, the out-of-plane current density is shown in Figure 3. According to panels in Figure 3, the maximum electrical current density is seen at the reconnection sites. As the shear flow velocity amplitude increases, the fragmentation of the current sheet and the growth rate of the plasmids decrease, and the current sheet retains its original structure for a longer time. Moreover, by increasing the shear flow velocity of the order of super-Alfvénic, the current density perturbations around the reconnection point are maximized. For example, for $V_0 = 15$ (fig.3(h)), these MHD perturbations are more conspicuous in the upstream regions, where the flow velocity is of the order of super-Alfvénic velocity than in the downstream regions, where the flow velocity is of the order of Alfvénic velocity. These perturbations are due to the KH instability when the shear velocity is greater than the Alfvénic limit. Hence, the maximum reconnection rate for different values of shear velocity in Figure 4 shows that the reconnection rate decreases with increasing V_0. When $V_0 = 1.5$, that means the shear ve-

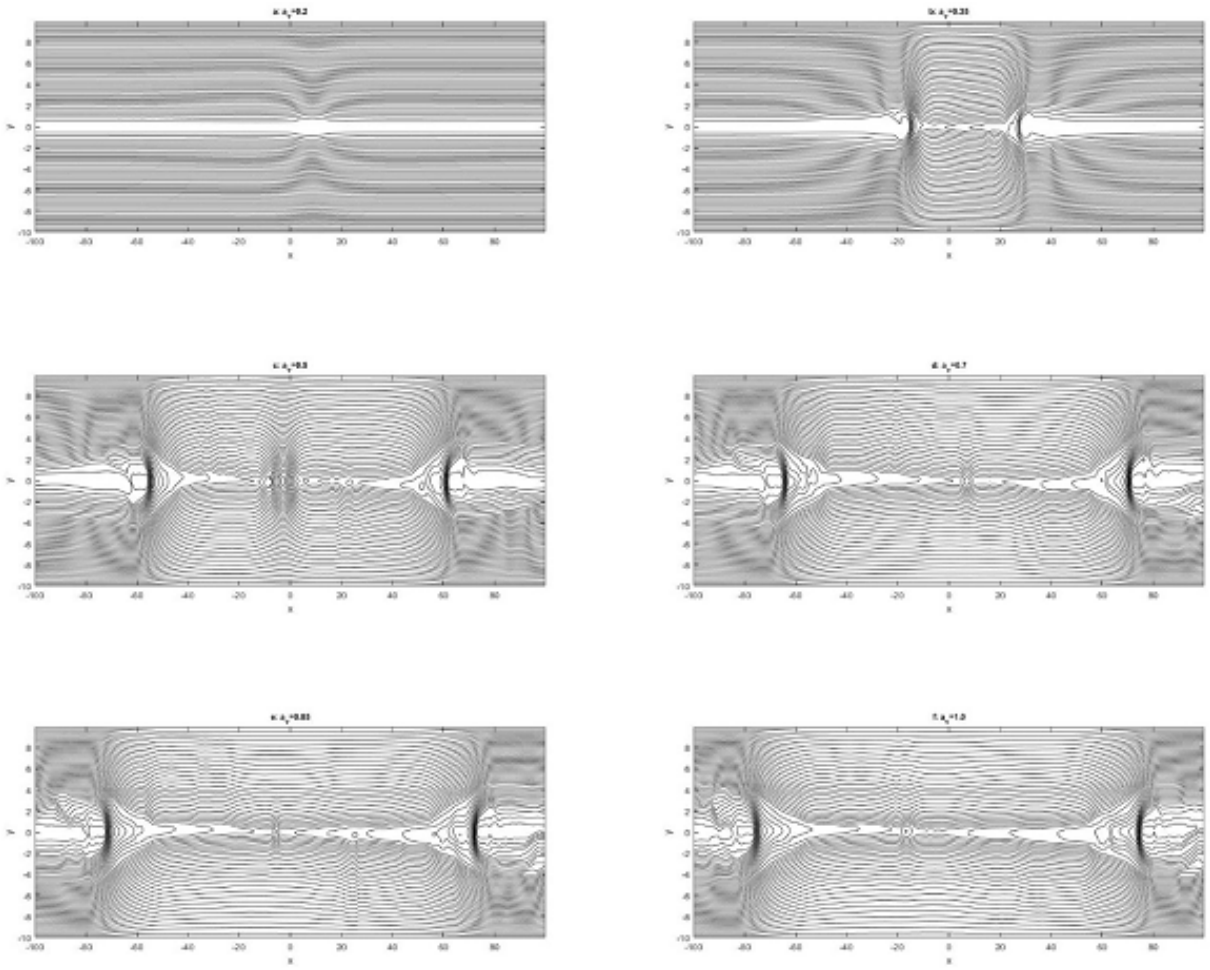

Figure 6. Force lines for different values of shear flow thickness at $t = 100\tau_A$, and $a_v =$ a)0.2 , b)0.35 , c)0.5 , d)0.7 , e)0.85 , f)1.

locities are of the order of Alfvénic or larger on both sides of the current sheet, the current sheet keeps its primary structure. This topic is in agreement with previous studies on the nonlinear tearing mode instability [42,43] in presence of symmetric shear flow. So that, the tearing mode instability is fully stabilized by Alfvénic velocity.

3.2 Varying shear flow thickness

In this section, we discuss the effect of different half-thickness of the shear flow on the evolution of the plasmoid instability. Here, we assume the shear flow velocity amplitude is fixed,$V_0 = 0.8V_A$, and the half-thickness of shear flow varies as $a_v = 0.2, 0.35, 0.5, 0.7, 0.85, 1.0, 1.25$.

Remember that the half-thickness of magnetic shear is $a_B = 0.7$. The half-thickness of the shear flow is considered as a significant parameter in the process of magnetic reconnection and plasmoid instability. The temporal variation of the reconnection rate in Figure 5 shows that for small values of $a_v = 0.2$, reconnection does not occur, and the linear phase of the system is larger, meaning that the system takes a long time to achieve instability. The magnetic field lines for different values of shear flow thickness are shown in Figure 6 at the same time ($t = 100\tau$). As seen from Figure 6(a), the plasmoid instability does not occur in a small value of $a_v = 0.2$, and the current sheet is stabilized against plasmoid instability. In the greater values of $a_v = 0.35, 0.5$, the reconnection and plasmoid instability are developed and the current sheet becomes unstable. Therefore, shear flow can have either boosting or suppressing effects on the plasmoid instability growth rate, which is predominantly determined by the shear flow thickness.

Figure 7 shows the maximum reconnection rate for different values of a_v, assuming the velocity amplitude is constant $V_0 = 0.8V_A$. The red dashed line represents the peak reconnection under conditions where the shear flow is perfectly anti-parallel to the background magnetic field (i.e $a_v = a_B$). When $a_v < a_B$ the peak reconnection rate decreases, while for $a_v > a_B$ the peak reconnection rate increases. In this simulation, we found a critical value for shear flow thickness in the presence of sub-Alfvénic asymmetric shear flow with ampli-

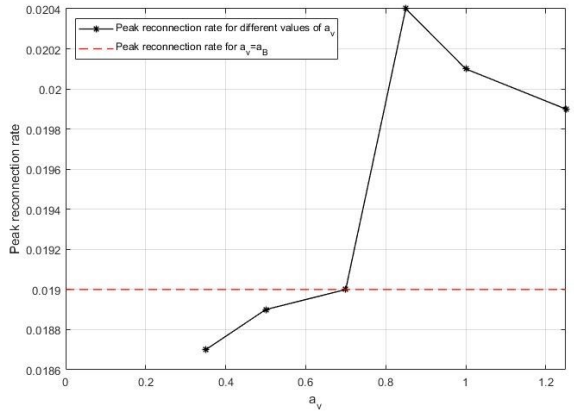

Figure 7. Peak reconnection rate for different values of a_v .

tude $V_0 = 0.8V_A$ in upstream and $V_0 = 0.6V_A$ in downstream. Therefore, maximum reconnection rate has been obtained at $a_{vc} = 0.85$ (i.e $a_{vc} = 1.2a_B$).

However, when the half-thickness of shear flow is greater than the critical thickness, the maximum reconnection rate or linear growth rate decreases, which means that the shear flow velocity can have either stabilized or destabilized effects on the plasmoid instability development dependent on the half-thickness of shear flow.

4. Summary

Using 2.5-dimensional MHD simulations, we investigated the effect of anti-symmetric parallel sheared plasma flow on the dynamics of plasmoid instability in a Harris current sheet. In these simulations, at very early times, we used a non-uniform localized resistivity to trigger fast reconnection at the origin. After that, a uniform resistivity was set. To investigate in more detail the effect of asymmetric sheared plasma flow on the non-linear evolution of the current layer, our study considered a wide range of parameters both for the shear flow velocity amplitude (sub-Alfvénic to super-Alfvénic) and the shear flow thickness.

The results showed that asymmetric sheared plasma flows with a thickness comparable to the magnetic shear length can lead to significant effects on magnetic reconnection and plasmoid instability. The presence of sub-Alfvénic shear flow causes the change of primary O-point (where high pressure and density plasma is enclosed,) position from the center of the current sheet. As the amplitude of the asymmetric shear flow velocity increases, the reconnection rate and the growth rate of plasmoid instability decreases, and also the linear phase of the system becomes longer. We also found that, in strong shear flows (Alfvénic limit), the Kelvin-Helmholtz instability prevails in the system instead of the plasmoid instability. Due to the fast growth of KH instability, magnetic field lines twist near the origin, and the reconnection structure deformed. Furthermore, super-Alfvénic shear flows can fully suppress the plasmid instability, and so, the initial configuration of the current sheet remains stable.

The sub-Alfvénic shear flow can have both boosting or suppressing effects on the plasmoid instability development, which is completely controlled by shear flow scale length (or shear flow thickness). In our study, the influence of different values of the shear flow thickness was investigated, with a sub-Alfvénic velocity. We found that, for small values of the thickness (here $a_v = 0.2$), the reconnection does not occur, and the current sheet remains stable. Thus, the reconnection rate or growth rate of plasmoid instability for $a_v < a_B$ is less than $a_v = a_B$ (an equilibrium state). Also, we found a critical value for the shear flow thickness at $a_v = 1.2a_B$ where the reconnection rate is maximum.

Conflict of interest statement:

The authors declare that they have no conflict of interest.

References

[1] Y. M. Huanga, L. Comisso, and A. Bhattacharjee. *The Astrophysical Journal*, **849**:75, 2017.

[2] A. Miura. *Physical review letters*, **49**:779, 1982.

[3] M. Hesse and P. A. Cassak. *Space Physics*, **125**:e2018JA025935, 2020.

[4] E. W. Hones Jr. *Eos, Transactions American Geophysical Union*, **65**:340, 1984.

[5] J. Ye, Q. Cai, C. Shen, J. C. Raymond, J. Lin, I. I. Roussev, and Z. Mei. *The Astrophysical Journal*, **987**:64, 2020.

[6] D. F. Webb and T. A. Howard. *Living Reviews in Solar Physics*, **9**:1, 2012.

[7] C. T. Russell. *IEEE transactions on plasma science*, **28**:1818, 2000.

[8] D. Biskamp. *The Physics of fluids*, **29**:1520, 1986.

[9] N. F. Loureiro, R. Samtaney, A. A. Schekochihin, and D.A. Uzdensky. *Physics of Plasmas*, **19**:042303, 2012.

[10] A. Bhattacharjee, Y. M. Huang, H. Yang, and B. Rogers. *Physics of Plasmas*, **16**:112102, 2009.

[11] H. Lotfi and M. Hosseinpour. *Frontiers in Astronomy and Space Sciences*, **8**, 2021.

[12] L. Ni, U. Ziegler, Y. M. Huang, J. Lin, and Z. Mei. *Physics of Plasmas*, **19**:072902, 2012.

[13] H. Baty. *Journal of Plasma Physics*, **80**:655, 2014.

[14] N. Ahmad, P. Zhu, A. Ali, and S. Zeng. *Plasma Science and Technology*, **24**:015103, 2022.

[15] L. Comisso and D. Grasso. *Physics of Plasmas*, **23**:032111, 2016.

[16] H. Baty, E. R. Priest, and T. G. Forbes. *Physics of plasmas*, **13**:022312, 2006.

[17] N. A. Murphy, M. P. Miralles, C. L Pope, J. C. Raymond, H. D. Winter, K. K. Reeves, D. B. Seaton, A. A. van Ballegooijen, and J. Lin. *The Astrophysical Journal*, **751**:56, 2012.

[18] C. E. Doss, C. M. Komar, P. A. Cassak, F. D. Wilder, S. Eriksson, and J. F. Drake. *Journal of Geophysical Research: Space Physics*, **120**:7748, 2015.

[19] L. Ni, J. Lin, and N. A. Murphy. *Physics of Plasmas*, **20**:061206, 2013.

[20] L. Wang, X. Q. Wang, X. G. Wang, and Y. Liu. *Chinese Physics B*, **23**:025203, 2013.

[21] J. Wang, X. Wang, and C. Xiao. *Physics Letters A*, **372**:4614, 2008.

[22] E. W. Hones Jr, J. R. Asbridge, S. J. Bame, M. D. Montgomery, S. Singer, and S-I. Akasofu. *Journal of Geophysical Research*, **77**:5503, 1972.

[23] E. W. Hones Jr and K. Schindler. *Journal of Geophysical Research: Space Physics*, **84**:7155, 1979.

[24] S. Wang, L. C. Lee, and C. Q. Wei. *Physics of fluids*, **31**:1544, 1988.

[25] T. Sato and R. J. Walker. *Journal of Geophysical Research: Space Physics*, **87**:7453, 1982.

[26] L. N. Wu and Z. W. Ma. *Physics of Plasmas*, **21**:072105, 2014.

[27] J. Wang, C. Liu, N. Deng, and H. Wang. *Astrophysical Journal*, **853**:143, 2018.

[28] G. Yang, Y. Xu, W. Caoa, H. Wang, C. Denker, and R. Rimmele Thomas. *Astrophysical Journal Letters*, **617**:L151, 2004.

[29] Na. Deng, Y. Xu, G. Yanga, W. Cao, C. Liu, R. Rimmele Thomas, H. Wang, and C. Denker. *Astrophysical Journal*, **644**:1278, 2006.

[30] W. Manchester. *Journal of Geophysical Research: Space Physics*, **108**:121688, 2003.

[31] R. Rankin, P. Frycz, J. C. Samson, and V. T Tikhonchuk. *Physics Review D*, **4**:829, 1997.

[32] J. C. Samson and R. Rankin. *Washington DC American Geophysical Union Geophysical Monograph Series*, **81**:253, 1994.

[33] J. H. Li and Z. W. Ma. *Journal of Geophysical Research: Space Physics*, **115**:162002, 2010.

[34] X. Zhang, L. J. Li, L. C. Wang nad J. H. Li, and Z. W. Ma. *Physics of Plasmas*, **18**:092112, 2011.

[35] M. Hosseinpour, Y. Chen, and S. Zenitani. *Physics of Plasmas*, **25**:102117, 2018.

[36] L. Ni, K. Germaschewskia, Y-M. Huang, B. P. Sullivan, H. Yang, and A. Bhattacharjee. *Physics of Plasmas*, **17**:052109, 2010.

[37] D. A. Knoll and L. Chac`òn. *Physical review letters*, **88**:215003, 2002.

[38] S. Zenitani. *Astrophysics Source Code Library (ASCL)*, :1604, 2016.

[39] T. Miyoshi and K. Kusano. *Journal of Computational Physics*, **208**:315, 2005.

[40] A. Dedner, F. Kemm, D. Kröner, C-D. Munz, T. Schnitzer, and M. Wesenberg. *Journal of Computational Physics*, **175**:645, 2002.

[41] T. Shimizu, K. Kondoh, and S. Zenitani. *Physics of Plasmas*, **24**:112117, 2017.